We are IntechOpen, the world's leading publisher of Open Access books Built by scientists, for scientists

4,800
Open access books available

122,000
International authors and editors

135M
Downloads

Our authors are among the

154
Countries delivered to

TOP 1%
most cited scientists

12.2%
Contributors from top 500 universities

CLARIVATE ANALYTICS BOOK CITATION INDEX INDEXED

WEB OF SCIENCE™

Selection of our books indexed in the Book Citation Index in Web of Science™ Core Collection (BKCI)

Interested in publishing with us?
Contact book.department@intechopen.com

Numbers displayed above are based on latest data collected.
For more information visit www.intechopen.com

Chapter 14

Resistive Electrothermal Sensors, Mechanism of Operation and Modelling

Heyd Rodolphe

Additional information is available at the end of the chapter

http://dx.doi.org/10.5772/60888

1. Introduction

The purpose of this chapter is to present the rich topic of resistive electrothermal sensors, from modelling to applications. Because of their manufacturing simplicity and ease of use, miniature resistive sensors are commonly used in many application fields, when the temperature or heat flux need to be measured. In flow metrology, the hot wires are commonly used to measure fast-changing flows for a wide range of velocities [2]. In biomedical instrumentation [3], due to their small size and the absence of moving parts, the resistive sensors can be used in vivo to accurately track real-time changes of blood flow and temperature.

In the present chapter we will focus on the study, the modelling and the applications of the most used resistive sensors, such as the resistance temperature detectors (RTD) made of a pure metal wire or a metallic thin film.

If on the one hand the electrical resistance of the sensor contains all the necessary information about its operating temperature, on the other hand it is essential that the sensor be traversed by an electric current in order to measure its resistance and then deduce its temperature. This electric current generates heat inside the sensor by the Joule effect and thus an unavoidable rise of its operating temperature. For the same values of the electrical parameters, this self-heating is more important as the sensor is small, and therefore this phenomenon is a major source of errors in the thermal measurements when using miniature resistive sensors. To quantify this deviation, sensors manufacturers usually measure a steady-state self-heating index (SHI) [4], that is only valid for one given operating temperature and one given surrounding environment, such as air or water for example.

Thus a realistic modelling of these sensors, based for example on electrothermal analogies [10] or on the use of thermal Laplace transfer functions [11], will allow to open new strategies

for a wider and a better use of these sensors in the fields of temperature or heat flux measurements, but also for the thermal characterization of materials. We will expose in this chapter a sytemic approach, that includes simultaneously and in a single mathematical environment: a realistic modelling of the sensors and of their interactions with the system under study, both of them being described by partial differential equations (PDEs); the modeling of power, control and signal processing systems, described by electrical circuits and thus ordinary differential equations (ODEs).

2. Metallic resistive sensors

2.1. Presentation

The metallic resistive sensors, often called resistance temperature detectors (RTDs), are widely used, as well in the industry (automotive, medical, food) as in the academic laboratories, either in the form of a pure thin metal wire or as a thin film. The possible configurations are numerous (single wire, wire wound, duplex configuration, encapsulated flat film) but in all the cases, the underlying mechanisms of operation are based on the heat transfer between the metallic sensor and the surrounding media to be sensed.

We present here two base configurations: the single wire (Fig. 1a) and the thin encapsulated flat film (Fig. 1b). The former is frequently used to characterize fluid flows, as in the case of the hot wire anemometer [1, 2], but also to measure the thermal properties of solids [5, 6] and liquids [7]. The latter is widely used to measure the temperature.

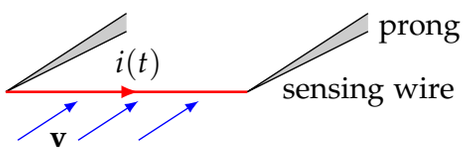

(a) Pure metal wire sensor used for flow measurement.

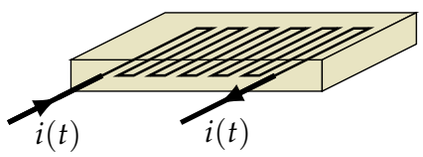

(b) Encapsulated pure metal flat film sensor.

Figure 1. Two base configurations of metallic resistive sensors commonly used in the industry and laboratories. The characteristic lengths are of the order of millimeters, the widths and the diameters in the micrometer range or less.

2.2. Modelling

2.2.1. General hypothesis – Mathematical model

The operation of the metallic resistive sensors is generally limited to a relatively narrow temperature range near a given operating point, such that the physical characteristics of the constitutive materials of the sensor can usually be assumed to be constant during operation. As an example, these sensors are commonly used to measure variations of temperature with an extent of less than 100 K, in the vicinity of the room temperature. Under these conditions, the radiative heat transfer between the sensor and its environment can also be neglected or eventually linearized. Thus a linear model is very adequate to describe the most usual modes of operation of these kinds of electrothermal sensor. Without loss of generality of the study, it is furthermore assumed here that the physical quantities describing the system only depend of time and solely of one space variable, denoted x. In the most general case, the

http://dx.doi.org/10.5772/60888

system has to be considered as composite, as in the case of the figure 1b, thus we denote by $T_j(x,t)$ the temperature inside the jth layer and by $\delta T_j(x,t)$ its variations compared to the room temperature T_a. For each of the layers constituting the sensor, it is possible to write a local energy balance equation in the general form:

$$\mu_j c_j \partial_t \left[\delta T_j(x,t)\right] \mathrm{d}\tau = k_j L_{x,j}(t) \left[\delta T_j(x,t)\right] \mathrm{d}\tau + \dot{w}_j(x,t)\mathrm{d}\tau \tag{1}$$

where μ_j, c_j and k_j are respectively the density, the specific heat and the thermal conductivity of the jth layer and $\mathrm{d}\tau$ is an infinitesimal volume element of this layer. We denote by $L_{x,j}(t)$ a differential operator linear in x, time-dependent, acting on $\delta T_j(x,t)$, and whose expression will be given later, according to the geometry of the considered sensor. The volume density of internal heat, $\dot{w}_j(x,t)$, appearing in the equation (1), is due to the Joule effect and is different from zero only inside the conductive elements of the sensor where an electric current is flowing. The boundary conditions accompanying the equation (1) depend of the mode of operation of the metallic sensor, and will be specified later.

At this stage, no hypothesis has been made about the electrical resistance of the sensor. We consider here two situations:

– In the case where the electric current is flowing in the same direction as the temperature gradient (figure 1a), it is mandatory to take into account the dependence of the electrical resistance with the x position. If $\mathrm{d}x$ denotes the length of an infinitesimal portion of the jth conductive material, its infinitesimal electrical resistance $dR_j(x,t)$ can be written as:

$$\mathrm{d}R_j(x,t) = r_j(x,t)\mathrm{d}x \tag{2}$$

where $r_j(x,t)$ is the lineic resistance. The average resistance $\overline{R}_j$ is then defined as $\overline{R}_j = \int_0^{\ell_j} r_j(x,t)\mathrm{d}x$, with ℓ_j the active length of the jth conductive material. In this case, the internal heat source takes the following form: $\dot{w}_j(x,t)\mathrm{d}\tau = i_j(t)^2 r_j(x,t)\mathrm{d}x$.

– In the case where the electric current is flowing in a direction perpendicular to that of the temperature gradient (figure 1b), we suppose that the resistance of the jth conductive layer is uniform and given by $R_j(t) = \ell_j r_j(t)$. In this case, the internal heat source takes the following form: $\dot{w}_j(x,t)\mathrm{d}\tau = i_j(t)^2 R_j(t)\mathrm{d}x/\ell_j = i_j(t)^2 r_j(t)\mathrm{d}x$.

In the vicinity of the ambient temperature, the lineic resistance of the metals commonly used in the formation of RTDs (such as Platinum, Nickel, Tungsten and even Silver), varies linearly with the temperature to a good approximation, making it possible to write this lineic resistance r_j as:

$$\begin{aligned} r_j(x,t) &= r_{j,\mathrm{ref}}\left[1 + \alpha_j\left(T_j(x,t) - T_{\mathrm{ref}}\right)\right] \\ &= r_{j,a} + \alpha_j r_{j,\mathrm{ref}} \delta T_j(x,t) \end{aligned} \tag{3}$$

where α_j is the temperature coefficient of the metal considered, T_{ref} is a reference temperature (usually $T_{\text{ref}} = 273.15$ K), $r_{j,a}$ and $r_{j,\text{ref}}$ are the values of the lineic resistance, respectively at the temperatures $T = T_a$ and $T = T_{\text{ref}}$. Using the relation (3) and writing $\mathrm{d}\tau = A_x \mathrm{d}x$, it is now possible to rewrite the source term $\dot{w}_j(x,t)\mathrm{d}\tau$ as:

$$\begin{aligned} \dot{w}_j(x,t)\mathrm{d}\tau &= r_{j,a} i_j(t)^2 \mathrm{d}x + \alpha_j r_{j,\text{ref}} i_j(t)^2 \delta T_j(x,t)\mathrm{d}x \\ &= \dot{w}_{j,a}(t)\mathrm{d}\tau + \alpha_j r_{j,\text{ref}} i_j(t)^2 \delta T_j(x,t)\mathrm{d}\tau / A_x \end{aligned} \tag{4}$$

The local energy balance can now be proposed in a form to be solved:

$$\mu_j c_j \partial_t \left[\delta T_j(x,t)\right] = \left(k_j L_{x,j}(t) + \frac{\alpha_j r_{j,\text{ref}}}{A_x} i_j(t)^2\right) \left[\delta T_j(x,t)\right] + \dot{w}_{j,a}(t) \tag{5}$$

The real-time mode of operation of the resistive sensor is obtained by solving the equations (5) for each layer. Depending on the time evolutions of both the electrical current $i_j(t)$ and of the boundary conditions, an analytical resolution of the equations (5) is unfortunately rarely possible. We will now discuss two possible ways to obtain a general solution of the differential equation describing the real-time evolution of the temperature inside the sensor: the method of Laplace transfer functions and an electrothermal analogy. Each of these methods presents some particular interests that will be exposed.

2.2.2. Transfer function approach – Inverse analysis

The resolution of the equations (5), by the approach in term of transfer functions, requires first of all be able to apply the Laplace transform to these equations. This is clearly impossible, firstly because of the time dependence of the $L_{x,j}(t)$ operator and secondly because of the term $i(t)^2$. However, in most cases considered in this study, we can decompose $L_{x,j}(t)$ in a stationary operator $L_{x,j}$ and a time-dependant part $a_{0,j}(t)$, independent of x:

$$L_{x,j}(t) = L_{x,j} + a_{0,j}(t) \tag{6}$$

It is thus possible to rewrite the equation (5) in the following form:

$$\mu_j c_j \partial_t \left[\delta T_j(x,t)\right] = k_j L_{x,j} \left[\delta T_j(x,t)\right] + a_j(t)\delta T_j(x,t) + \dot{w}_{j,a}(t) \tag{7}$$

where $a_j(t) = k_j a_{0,j}(t) + \alpha_j r_{j,\text{ref}} i_j(t)^2 / A_x$. Using the following change in function $\delta T_j(x,t) = f_j(t) u_j(x,t)$, and provided that $f_j(t) \neq 0 \ \forall t$, it is possible to transform the equation (7) in:

$$\mu_j c_j \partial_t \left[u_j(x,t)\right] = k_j L_{x,j} \left[u_j(x,t)\right] + \left[a_j(t) - \mu_j c_j \frac{f_j'(t)}{f_j(t)}\right] u_j(x,t) + \frac{\dot{w}_{j,a}(t)}{f_j(t)} \tag{8}$$

http://dx.doi.org/10.5772/60888

It is now possible to cancel the term $u_j(x,t)$ and thus obtain a differential equation with constant coefficients, provided to choose the function $f_j(t)$ such that $\mu_j c_j f_j'(t)/f_j(t) = a_j(t)$. It is also possible to write this condition as follows:

$$f_j(t) = f_j(0) \exp \int_0^t \frac{a_j(\tau)}{\mu_j c_j} \mathrm{d}\tau \tag{9}$$

By choosing $f(0) = 1$, the differential equation (8) can finally be written in the form:

$$\mu_j c_j \partial_t \left[u_j(x,t)\right] = k_j L_{x,j} \left[u_j(x,t)\right] + \dot{w}_{j,a}(t) \exp \left[-\int_0^t \frac{a_j(\tau)}{\mu_j c_j} \mathrm{d}\tau\right] \tag{10}$$

The differential equation (10) satisfied by $u_j(x,t)$ has constant coefficients, thus it is now possible to apply the Laplace transform. By noting $s_j(t) = \dot{w}_{j,a}(t) \exp \left[-\int_0^t \frac{a_j(\tau)}{\mu_j c_j} \mathrm{d}\tau\right]$, $S_j(p) = \mathrm{TL}[s_j(t)]$ and $U_j(x,p) = \mathrm{TL}[u_j(x,t)]$, where TL is the Laplace transform and p is the Laplace variable, we obtain an ordinary differential equation (ODE) of the form:

$$\mu_j c_j \left(pU_j(x,p) - u_j(x,0)\right) = k_j L_{x,j} \left[U_j(x,p)\right] + S_j(p) \tag{11}$$

Examples of resolution of (11) will be given in the next sections with different expressions of the linear operator $L_{x,j}$ and $S_j(p)$.

The main advantage of the present approach is to allow to write the response $\delta T_j(x,t)$ of the jth layer in term of a Laplace function transfer $H_j(x,p)$, deduced from the resolution of the ODE (11). This opens the route to the inverse analysis of thermal signals [8–10] and to new sensors exploitation [2], as it will be shown later in this study. Unfortunately this approach is limited to the description of the linear mode of operation of the RTDs.

2.2.3. Electrothermal analogy – SPICE modelling

The previous approach is limited to the case of linear differential operators $L_{x,j}$ and constant physical properties. If we need to investigate larger temperature variations than previously assumed, the hypotheses of constant physical properties and linear operator are no more valid and we need another approach to be able to describe extreme operating modes of the RTDs. We present now a modelling of the resistive sensor based on an electrothermal analogy deduced from the Godunov's scheme. Let's consider an infinitesimal volume of the jth layer, as represented in figure 2a. This infinitesimal system, which is assumed opaque and undeformable, is on the one hand subjected to various elementary heat flows: axial heat conduction $\dot{q}_{c,j}$, a lateral heat transfer $\dot{q}_{\mathrm{lat},j}$ which may for example include a conducto-convective transfer $\dot{q}_{cc,j}$ or a radiative transfer $\dot{q}_{r,j}$. On the other hand this infinitesimal system may be subjected to an internal heat source $\dot{w}_j$ due to the Joule effect. Using the first law of thermodynamics, the energy balance of this infinitesimal system can be written as:

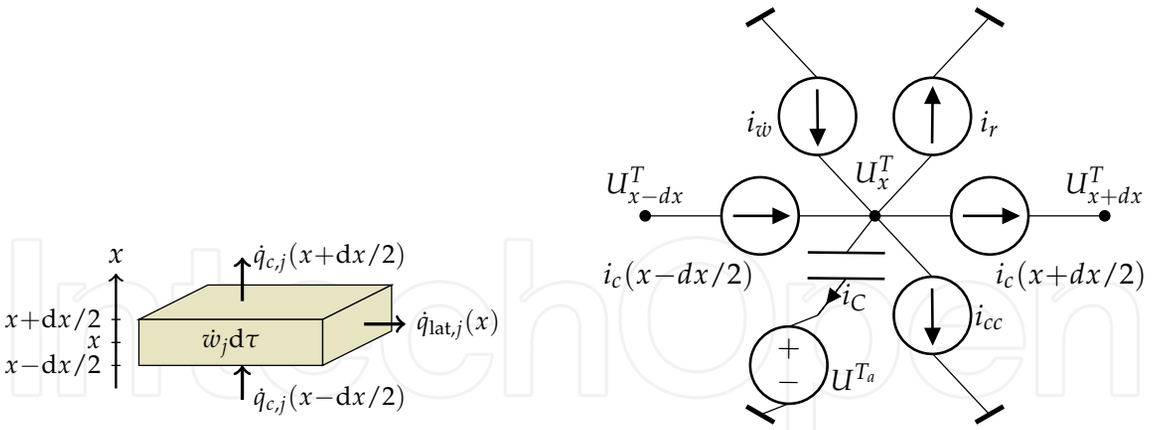

(a) Energy balance over an infinitesimal volume $\mathrm{d}\tau$.

(b) Electrothermal circuit equivalent to the infinitesimal system of the figure (a).

Figure 2. Balance of energy transfers inside an infinitesimal volume element $\mathrm{d}\tau$ of the jth layer and electrothermal analogy.

$$\mu_j c_j \partial_t T_j(x,t)\mathrm{d}\tau = \dot{w}_j(x,t)\mathrm{d}\tau + \dot{q}_{c,j}(x-\mathrm{d}x/2,t) + \dot{q}_{c,j}(x+\mathrm{d}x/2,t) + \dot{q}_{\mathrm{lat},j}(x,t) \qquad (12)$$

where the elementary heat fluxes are given by:

- $\dot{q}_{c,j}(x-\mathrm{d}x/2) = -A_x(k_j\partial_x T_j)_{x-\mathrm{d}x/2} = A_x j_{c,j}(x-dx/2)$ and $\dot{q}_{c,j}(x+\mathrm{d}x/2) = A_x(k_j\partial_x T_j)_{x+\mathrm{d}x/2} = -A_x j_{c,j}(x+dx/2)$. The partial derivative $(\partial_x T_j)_{x-\mathrm{d}x/2}$ is approximated by $[T_j(x,t)-T_j(x-\mathrm{d}x,t)]/\mathrm{d}x$ and $(\partial_x T_j)_{x+\mathrm{d}x/2}$ by $[T_j(x+\mathrm{d}x,t)-T_j(x,t)]/\mathrm{d}x$.
- The elementary lateral heat flux may take several forms, depending on the lateral boundary conditions. It may include for example:
  - a radiative term $\dot{q}_{r,j}(x) = -\sigma\varepsilon_j\left[T_j^4(x,t)-T_a^4\right]A_{\mathrm{lat}} = -j_{r,j}(x)A_{\mathrm{lat}}$, where σ is the Stefan-Boltzmann constant, ε_j the emissivity of the material and A_{lat} the lateral area of exchange.
  - a conducto-convective term $\dot{q}_{cc,j}(x) = -h_j\left[T_j(x,t)-T_a\right]A_{\mathrm{lat}} = -j_{cc,j}(x)A_{\mathrm{lat}}$, where h_j is the Newton coefficient of exchange.

We now introduce the following unsteady electrothermal analogy, which consists in the associations shown in Table 1.

thermal quantity	temperature or temperature variations (K)	thermal capacity ($\mathrm{J.K^{-1}}$)	elementary heat flux (W)	internal heat source (W)
	T or δT	$\mu c\mathrm{d}\tau$	jA	$\dot{w}\mathrm{d}\tau$
electrical analogy	V^T or U^T	C	i	$i_{\dot{w}}$
	potentiel or tension (V)	capacity ($\mathrm{C.V^{-1}}$ or F)	intensity (A)	intensity (A)

Table 1. Unsteady electrothermal analogy used to model RTDs.

http://dx.doi.org/10.5772/60888

By introducing the surface heat fluxes j, it is possible to rewrite the equation (12) as:

$$\begin{aligned}\mu_j c_j \partial_t T_j(x,t)\mathrm{d}\tau = \dot{w}_j(x,t)\mathrm{d}\tau + j_{c,j}(x-\mathrm{d}x/2,t)A_x - j_{c,j}(x+\mathrm{d}x/2,t)A_x \\ - j_{r,j}(x,t)A_{\mathrm{lat}} - j_{cc,j}(x,t)A_{\mathrm{lat}}\end{aligned} \tag{13}$$

Using the electrothermal analogy of the table 1, we can now rewrite an electrical version of the equation (13):

$$-C_j \partial_t U_j^T(x,t) + i_{\dot{w}_j}(x,t) + i_{c,j}(x-\mathrm{d}x/2,t) - i_{c,j}(x+\mathrm{d}x/2,t) - i_{cc,j}(x,t) - i_{r,j}(x,t) = 0 \tag{14}$$

Recalling that the current charge of a capacitor is written as $i_C(t) = C\partial_t U$, we can see that the balance equation (14) is equivalent to the Kirchhoff's current law, applied to the node x of the portion of the electrothermal circuit represented in figure 2b:

$$-i_{C_j}(x,t) + i_{\dot{w}_j}(x,t) + i_{c,j}(x-\mathrm{d}x/2,t) - i_{c,j}(x+\mathrm{d}x/2,t) - i_{cc,j}(x,t) - i_{r,j}(x,t) = 0 \tag{15}$$

The controlled current sources, used in the electrothermal circuit of the figure 2b, are easily implemented in SPICE, allowing for a very complete systemic approach of the operation of the RTDs sensors, even in the case of extreme nonlinear conditions. Using this approach, it is possible to simulate the complete operation of the resistive sensor, from the heat transfer between the sensor and its environment to the instrumentation circuits. Unfortunately this analogy doesn't allow the same inverse analysis possibilities than those offered by the transfer function approach.

2.3. Resistive wire sensor

2.3.1. Presentation – Mathematical model

The hot-wire sensor is commonly used in anemometry and in flows characterization (HWA, see Fig. 3) as well as for the thermal characterization of fluids (THW, see Fig. 3b). This sensor is usually made of a metallic resistive wire with a diameter d of the order of a few microns and a length $\ell \gg d$, of the order of a few millimeters (Fig. 1a). This wire is heated by the Joule effect, due to the flow of an electric current of intensity $i(t)$ across the wire. The operating principle of this sensor is based on the balance between the energy supplied to the wire by the Joule heating and the energy lost by conduction, convection and radiation. The instantaneous average temperature $\overline{T}_{\mathrm{w}}(t)$, that is reached by the heated wire, is an image of the flow velocity and thermal characteristics of the fluid, that are to be measured. In general, the wire temperature is determined via the measurement of its instantaneous electrical resistance $\overline{R}_{\mathrm{w}}(t)$.

It is mainly the radial boundaries conditions, at $r = d/2$, that distinguish the two modes of operation of the single resistive wire sensor. In the domain of anemometry, the conducto-convective boundary conditions are considered, while in the domain of thermal characterization it is rather the conductive boundary conditions that are taken into account. In this last case the convection is considered as an obstacle to the measure, and should be minimized.

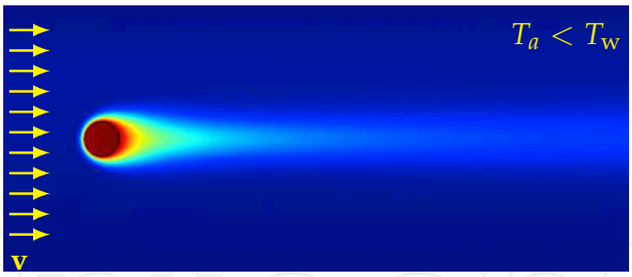

(a) HWA mode. Visualization of the temperature T_w of the hot wire and T_f of the fluid (atmospheric air is considered here), in a transverse plane x = cste. The temperature is calculated by the finite element technique using the code OpenFoam. **v** is the velocity of the fluid far away from the stationary wire.

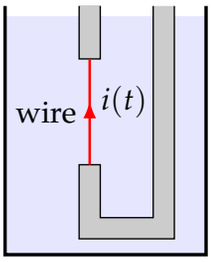

(b) THW mode. Hot wire immersed in a fluid, for an utilization in thermal characterization mode.

Figure 3. Different modes of operation of a single metallic wire: (a) Hot Wire Anemometry (HWA) and (b) Transient Hot Wire method. The temperature of the fluid, far away from the wire, is denoted by T_a.

As the sensor is only made by one material, here $j = 1$ and T_w will denote the wire temperature. In the most general case, the temperature of the wire can be written in the form $T_w = T_w(r, \theta, x, t)$. However, we can examine the dependence of T_w with the different space variables. According to the resolution by finite element shown in Fig. 3 and due to the very small diameter of the wire, we can see that the temperature of the wire presents the axial symmetry and is independent of r. In conclusion we can suppose to a very good approximation that the temperature of the wire only depends on the axial variable x and the time t : $T_w = T_w(x, t)$. The characteristic diameter of the holders being substantially greater than the one of the sensitive wire, their electrical resistances are perfectly negligible compared to the electric resistance $\overline{R}_w(t)$ of the wire, therefore only the latter is subjected to a significant temperature rise by the Joule effect. The supports must then be considered as cold heat sinks with a constant temperature, equal to that of the ambient temperature (or measurement temperature) T_a.

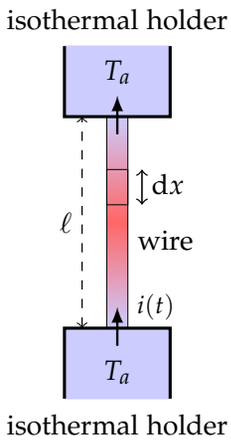

(a) Axi-symmetric modelling of a resistive hot wire with diameter d and length ℓ.

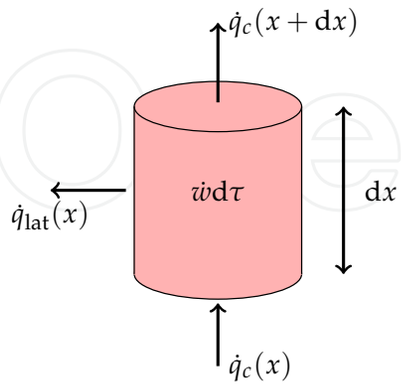

(b) Energy balance of an infinitesimal volume element of the hot wire $\mathrm{d}\tau = A_x \mathrm{d}x$.

Figure 4. Axi-symmetric modelling of a single hot wire. The diameter d of the wire is much smaller than the one of the holders.

The energy balance of an infinitesimal volume element $\mathrm{d}\tau$ of the hot wire is written in the general form (12), where $\dot{q}_{\mathrm{lat}}(x)$ depends on the mode of operation of the sensor. For example:

- In the HWA mode: $\dot{q}_{\mathrm{lat}}(x) = \dot{q}_r(x) + \dot{q}_{cc}(x)$;
- In the THW mode: $\dot{q}_{\mathrm{lat}}(x) = \dot{q}_{cm}(x)$, where the letter m indicates that the conduction has to be considered in the surrounding medium and the radiative contribution is negligible;
- In a fuse mode: $\dot{q}_{\mathrm{lat}}(x) \approx 0$.

2.3.2. Linear mode of operation – A new HWA method

2.3.2.1. HWA modelling

We focus here on the HWA modelling in the linear regime. In this case, the approach in terms of transfer functions will allow to propose a new method for the absolute measurement of the fluids flow velocity [2]. Under the assumptions of the linear regime, the balance equation (5) becomes in this case:

$$\mu_{\mathrm{w}} c_{\mathrm{w}} \partial_t \left[\delta T_{\mathrm{w}}(x,t)\right] = \left(k_{\mathrm{w}} \partial_{x^2} - h(v)\frac{\pi d}{A_x} - 4\sigma\varepsilon_{\mathrm{w}} T_a^3 \frac{\pi d}{A_x} + \frac{\alpha_{\mathrm{w}} r_{\mathrm{w,ref}}}{A_x} i(t)^2\right)\left[\delta T_{\mathrm{w}}(x,t)\right] + \dot{w}_a(t) \tag{16}$$

where $A_x = \pi d^2/4$, T_a is the temperature of the fluid far from the wire and is assumed constant, ε_{w} is the emissivity of the wire and $h(v)$ is the Newton coefficient of exchange, which value depends on the velocity amplitude v of the fluid far from the wire. We assume that the direction of the flow is perpendicular to the symmetry axis of the wire (see Fig. 3). It is also possible to introduce the Nusselt number Nu defined by $h(v) = k_f \mathrm{Nu}(v)/d$, where k_f is the thermal conductivity of the fluid:

$$\mu_{\mathrm{w}} c_{\mathrm{w}} \partial_t \left[\delta T_{\mathrm{w}}(x,t)\right] = \left(k_{\mathrm{w}} \partial_{x^2} - \mathrm{Nu}(v)\frac{\pi k_f}{A_x} - 4\sigma\varepsilon_{\mathrm{w}} T_a^3 \frac{\pi d}{A_x} + \frac{\alpha_{\mathrm{w}} r_{\mathrm{w,ref}}}{A_x} i(t)^2\right)\left[\delta T_{\mathrm{w}}(x,t)\right] + \dot{w}_a(t) \tag{17}$$

From the equation (17) we can identify the linear differential operator $L_{x,\dot{w}}(t)$ of the equation (5) as:

$$L_{x,\dot{w}}(t) = k_{\mathrm{w}} \partial_{x^2} - \mathrm{Nu}(v)\frac{\pi k_f}{A_x} - 4\sigma\varepsilon_{\mathrm{w}} T_a^3 \frac{\pi d}{A_x} \tag{18}$$

where the time dependence of $L_{x,\dot{w}}(t)$ is generally due to the time variations of the speed v. We assume now that the speed v of the fluid is constant and that the variations δT_{w} of the temperature of the wire are small compared to $1/\alpha_{\mathrm{w}}$ (which is of the order of 300 K). This last assumption allows to neglect the term $\alpha_{\mathrm{w}} r_{\mathrm{w,ref}} i(t)^2 \delta T_{\mathrm{w}}(x,t)/A_x$ compared to the term $\dot{w}_a(t)$, assuming that $r_{\mathrm{w,ref}} \approx r_{\mathrm{w},a}$, which is easy to realize. Under these assumptions, the equation (17) can be rewritten as:

$$\mu_{\mathrm{w}} c_{\mathrm{w}} \partial_t \left[\delta T_{\mathrm{w}}(x,t)\right] = \left(k_{\mathrm{w}} \partial_{x^2} - \mathrm{Nu}(v)\frac{\pi k_f}{A_x} - 4\sigma\varepsilon_{\mathrm{w}} T_a^3 \frac{\pi d}{A_x}\right)\left[\delta T_{\mathrm{w}}(x,t)\right] + \dot{w}_a(t) \tag{19}$$

The Laplace transform TL can now be directly applied to this equation. By denoting $\Theta_{\mathrm{w}}(x,s) = \mathrm{TL}[\delta T_{\mathrm{w}}(x,t)]$ and $\dot{W}_a(s) = \mathrm{TL}[\dot{w}_a(t)]$, we get the following ODE:

$$\begin{aligned}\mu_{\mathrm{w}} c_{\mathrm{w}} \left(s\Theta_{\mathrm{w}}(x,s) - \delta T_{\mathrm{w}}(x,0)\right) = k_{\mathrm{w}} \frac{\mathrm{d}^2}{\mathrm{d}x^2}\Theta_{\mathrm{w}}(x,s) \\ - \left(\mathrm{Nu}(v)\frac{\pi k_f}{A_x} + 4\sigma\varepsilon_{\mathrm{w}} T_a^3 \frac{\pi d}{A_x}\right)\Theta_{\mathrm{w}}(x,s) + \dot{W}_a(s)\end{aligned} \tag{20}$$

We assume the usual initial condition $\delta T_{\mathrm{w}}(x,0) = 0$ and isothermal boundary conditions $\delta T_{\mathrm{w}}(x = \pm\ell/2, t) = 0$, recalling that the holders are supposed to be isothermal. Using this assumptions, the solution of (20) is given by:

$$\Theta_{\mathrm{w}}(x,s) = \frac{\dot{W}(s)}{\beta + \frac{k_{\mathrm{w}}}{\kappa_{\mathrm{w}}}s}\left[1 - \frac{\cosh\left(\sqrt{s/\kappa_{\mathrm{w}} + \beta/k_{\mathrm{w}}}\, x\right)}{\cosh\left(\sqrt{s/\kappa_{\mathrm{w}} + \beta/k_{\mathrm{w}}}\, \ell/2\right)}\right] = H_{\mathrm{w}}(x,s) \times \dot{W}(s) \tag{21}$$

where $\dot{W}(s) = \dot{W}_a(s)/\mu_{\mathrm{w}} c_{\mathrm{w}} = \kappa_{\mathrm{w}}\dot{W}_a(s)/k_{\mathrm{w}} = 4\kappa_{\mathrm{w}} r_{\mathrm{w},a}\mathrm{TL}[i(t)^2]/\pi d^2 k_{\mathrm{w}}$, $x \in [-\ell/2, \ell/2]$ and $\beta = 4k_f \mathrm{Nu}/d^2 + 16\sigma\varepsilon_{\mathrm{w}} T_a^3/d$. The solution (21) has the form of the product of a transfer function $H_{\mathrm{w}}(x,s)$ by an excitation signal $\dot{W}(s)$. Therefore, this approach allows to model the infinitesimal volume $\mathrm{d}\tau$ of the hot wire, in the form of a linear system described by the transfer function $H_{\mathrm{w}}(x,s)$, as shown in Fig. 5.

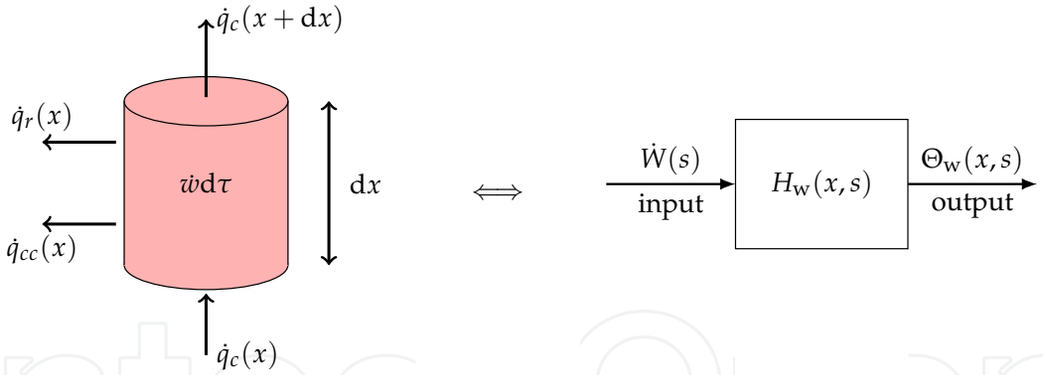

Figure 5. Linear modelling of an infinitesimal volume of the hot wire in HWA mode.

In practice, by measuring the resistance of the hot wire, one reaches the average temperature $\delta\overline{T}_{\mathrm{w}}(t) = \overline{T}_{\mathrm{w}}(t) - T_a$ of the wire rather than that of the sections of the wire. One can however obtain the expression of the average Laplace temperature $\overline{\Theta}_{\mathrm{w}}(s)$ by using the average transfer function $\overline{H}_{\mathrm{w}}(s)$ of the wire, defined by:

$$\overline{H}_{\mathrm{w}}(s) = \frac{1}{\ell}\int_{-\ell/2}^{\ell/2} H_{\mathrm{w}}(x,s)\mathrm{d}x = \frac{1}{\beta + \frac{k_{\mathrm{w}}}{\kappa_{\mathrm{w}}}s}\left[1 - \frac{\tanh\left(\sqrt{s/\kappa_{\mathrm{w}} + \beta/k_{\mathrm{w}}}\, \ell/2\right)}{\sqrt{s/\kappa_{\mathrm{w}} + \beta/k_{\mathrm{w}}}\, \ell/2}\right] \tag{22}$$

http://dx.doi.org/10.5772/60888

The average temperature $\delta\overline{T}_{\mathrm{w}}(t)$ of the whole wire is then calculated by the Laplace inversion of the product $\overline{H}_{\mathrm{w}}(s) \times \dot{W}(s)$: $\delta\overline{T}_{\mathrm{w}}(t) = \mathrm{TL}^{-1}[\overline{H}_{\mathrm{w}}(s) \times \dot{W}(s)]$.

2.3.2.2. A new HWA method

The analysis of the expression (22) shows that, in the case of the linear regime with small temperature variations, the average function transfer $\overline{H}_{\mathrm{w}}(s)$ is independent of the excitation current $i(t)$ that flows through the wire, but depends only on the physical characteristics of the wire, of the fluid and of the flow. This observation is at the origin of a new absolute method of fluid flow characterization. Until now, the usual modes of operation of the hot wire anemometers consisted in measuring the amplitude of the average temperature of the wire, in response to a given flow velocity (or Nusselt number), using different forms of excitation currents. Previously, there were mainly two types of anemometers:

The constant current anemometer (CCA): schematically, the current intensity $i(t)$ through the wire is maintained constant (using an appropriate electrical circuit) and the variations of the wire temperature $\delta\overline{T}_{\mathrm{w}}(t)$, induced by the changes in the flow velocity, are measured via the corresponding variations $\delta\overline{R}_{\mathrm{w}}(t)$ of the resistance.

The constant temperature anemometer (CTA): in this case the average temperature of the wire is maintained constant (and thus the resistance is also maintained constant) by varying the intensity of the electrical current flowing through the wire, in response to the variations of the flow velocity.

The major drawback of these traditional utilization modes of the HWA is the need to calibrate the anemometer, since the amplitude of the temperature of the wire then depends directly on the amplitude of the excitation current. The new approach exposed here is very different[1] from the previous ones. By modelling the hot wire in terms of a Laplace transfer function, it is possible to easily examine the behavior of the wire in an domain that has not been yet visited: the frequency domain. We have plotted in Fig. 6 the evolution of the normalized imaginary part $\Im[\overline{H}_{\mathrm{w}}/\overline{H}_{\mathrm{w}}(0)]$ and the real part $\Re[\overline{H}_{\mathrm{w}}/\overline{H}_{\mathrm{w}}(0)]$ of the transfer function (22) in the Fourier space, by putting $s = 2\mathrm{i}\pi\nu_w$, where ν_w is the frequency of the heat source. The modeled wire is supposed to be made of platinum, with a length $\ell = 10$ mm and a diameter $d = 50\,\mu$m. The fluid considered here is the atmospheric air, flowing at room temperature with a velocity $v = 4\,\mathrm{m.s}^{-1}$, corresponding to a Nusselt number $\mathrm{Nu} = 2.1$.

As we can see from Fig. 6, the imaginary part of the transfer function shows a maximum value. The corresponding frequency $\nu_{w,m}$ depends only on the flow velocity, on the physical characteristics of the wire and of the fluid, but in any case not of the amplitude of the excitation, assuming that the wire is operating in its linear mode. Once the physical characteristics of the wire and the fluid are known, it becomes possible, using this new approach, to measure the velocity of the fluid in an absolute way, without the need of a prior calibration of the anemometer.

In order to experimentally access to the transfer function $\overline{H}_{\mathrm{w}}$ of the wire, the sensor has to be excited by an harmonic current $i(t) = \hat{I}\cos\omega t$ with a frequency $\nu = \omega/2\pi$, then we measure the corresponding harmonic variations of the temperature, at a frequency $\nu_w = 2\nu$.

[1] The usage that can be done of this new approach is also very different from the previous ones.

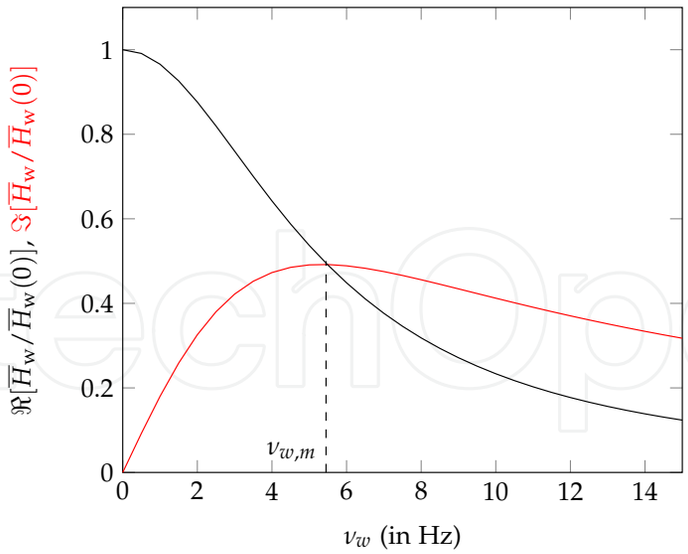

Figure 6. Evolution of the imaginary part $\Im[\overline{H}_w]$ and the real part $\Re[\overline{H}_w]$ of the transfer function (22) as a function of the frequency ν_w of the heat source, This example corresponds to the case of a platinum wire and atmospheric air at room temperature.

The Joule effect developed in the wire generates an averaged temperature oscillation $\delta\overline{T}_w(t)$ that contains a 2ω component written as $\delta\overline{T}_{2\omega}(t) = \Delta\hat{T}^0_{2\omega}(\nu)\cos 2\omega t + \Delta\hat{T}^q_{2\omega}(\nu)\sin 2\omega t$. Since the resistance of the wire is a known function of the temperature, the voltage drop $u(t) = \overline{R}_w(t)i(t)$ across the wire contains a 3ω component written as $u_{3\omega}(t) = \hat{U}^0_{3\omega}(\nu)\cos 3\omega t + \hat{U}^q_{3\omega}(\nu)\sin 3\omega t$. From equation (3) we can express the average resistance of the wire $\overline{R}_w(t)$ as:

$$\begin{aligned}\overline{R}_w(t) &= \int_{-\ell/2}^{\ell/2} r_w(x,t)\mathrm{d}x \\ &= R_{w,a} + \alpha_w R_{w,\mathrm{ref}}\delta\overline{T}_w(t) \\ &= R_{w,a} + \delta\overline{R}_w(t)\end{aligned} \tag{23}$$

The measurement of the harmonic variations $\delta\overline{T}_{2\omega}(t)$ of the temperature of the wire is achieved through the accurate measurement of the small harmonic component of the resistance variations $\delta\overline{R}_w(t)$.

There are mainly two kinds of circuits to achieve these measurements, the one that uses the classic Wheatstone bridge [2] and another one that uses a voltage divider (Fig. 7). This circuit must be balanced first, without any flowing, for each measurement temperature T_a, by ensuring that $R_g = R_{w,a}$ and thus $v(t) = 0$. Under flowing conditions, the use of two differential amplifiers allows to extract the informative signal $\Delta u(t) = u_1(t) - u_2(t)$ which is a function of $\delta\overline{T}_{2\omega}(t)$, the averaged harmonic temperature change of the line. The amplitude of $\Delta u(t)$ is very small in the linear regime and needs to be amplified by a factor $G \approx 1000$ using an instrumentation amplifier (IA). A dual phase synchronous detector (DPSD), adjusted to the third harmonic 3ω, allows to extract the amplitudes $\Delta\hat{T}^0_{2\omega}(\nu)$ and $\Delta\hat{T}^q_{2\omega}(\nu)$ from the voltage $v(t) = \alpha_w G\hat{I}R_{w,\mathrm{ref}}\delta\overline{T}_w(t)\cos\omega t$ delivered by the circuit.

http://dx.doi.org/10.5772/60888

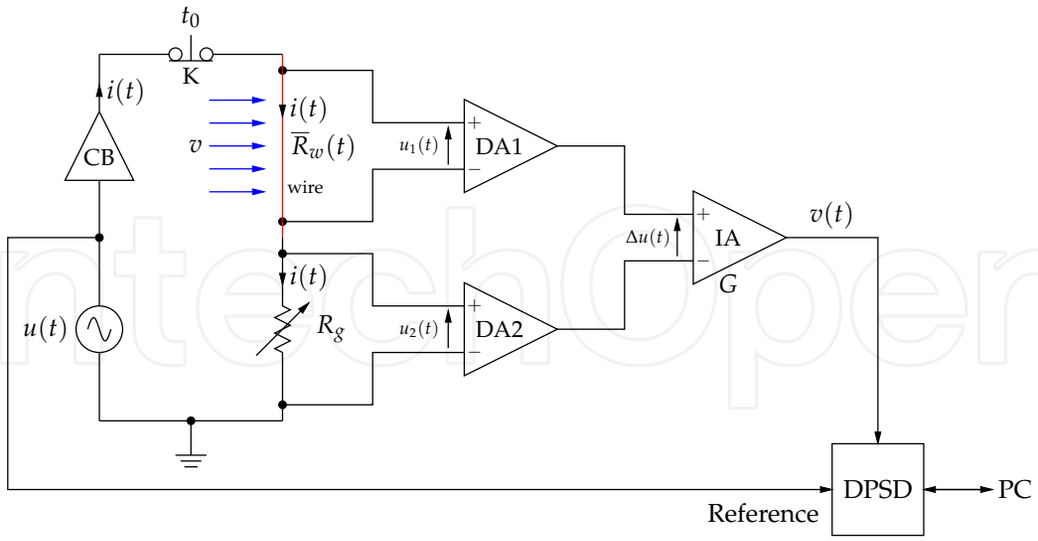

Figure 7. Circuit diagram of an experimental setup used for 3ω absolute anemometry. DPSD is a dual phase synchronous detector, that allows easy measurement of the 3ω harmonics real and imaginary parts. CB is a current buffer (LT1010), DA1 and DA2 are differential amplifiers (AMP03) and IA is an instrumentaion amplifier (AD620). The DPSD, controlled by a PC, is operating in the frequency sweep mode and third harmonic detection.

Figure 8 compares the theoretical real part (dashed line) and imaginary part (continuous line) of the transfer function (22) to measurements (squares and circles) of the 2ω temperature amplitudes, at different excitation frequencies, in the case of air flowing at a speed $v = 4\,\mathrm{m.s}^{-1}$ with ambient conditions, using a platinum wire of radius 25 μm, length $\ell = 1$ cm and a current amplitude $\hat{I} = 10$ mA. The results are plotted as a function of the frequency ν of the excitation current, that is half the heat source frequency: $\nu = \nu_w/2$.

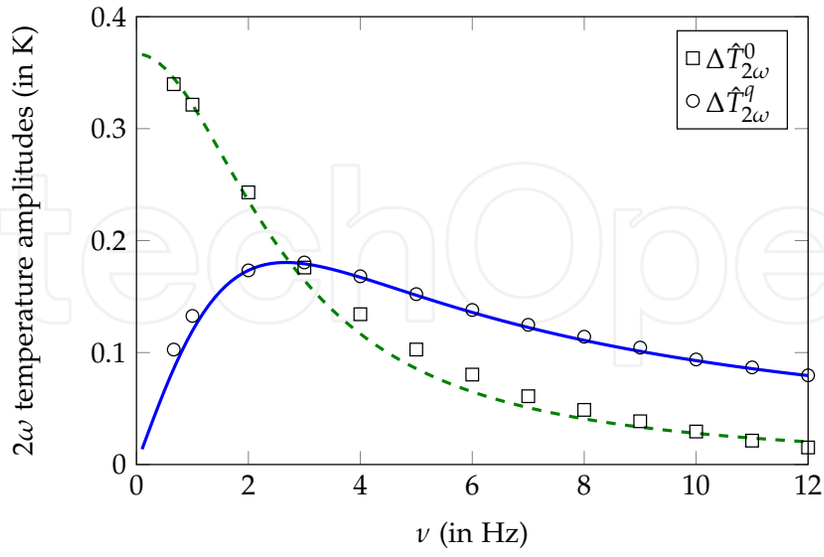

Figure 8. Experimental data (symbols) and theoretical results (lines) corresponding to the transfer function (22), with an air flow of spped $v = 4\,\mathrm{m.s}^{-1}$, at ambient temperature and pressure. The results were obtained in the case of a platinum wire of length $\ell = 1$ cm and radius $d/2 = 25\,\mu$m.

From the experimental results shown in Fig. 8, we found here $\nu_m^{\exp} = 2.67$ Hz, which is very close to the theoretical value $\nu_m = 2.70$ Hz predicted by the function transfer of the wire Eq. (22), Fig. 6 and Fig. 8. Using this approach, we have repeated the measurements of $\nu_m^{\exp}$ for different flow velocities v, and plotted the results as a function of v (Fig. 9).

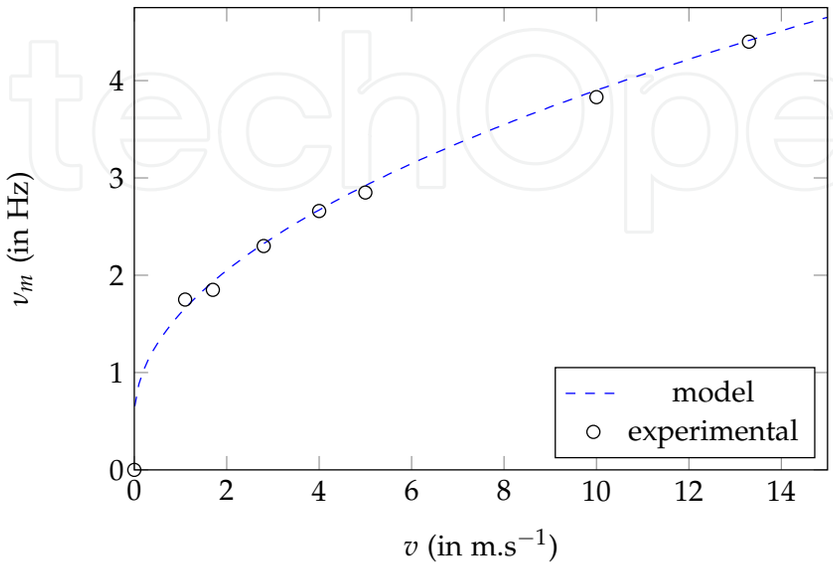

Figure 9. Absolute measurement of fluid velocity. The dashed line corrsponds to the calculation of ν_m by using the averaged transfer function (22).

As it can be seen on the figure 9, there is a good correspondence between the experimental values of the frequencies ν_m and the theoretical values (dashed line) calculated from the averaged transfer function (22), and using the Churchill's correlation (24). These results show that it is possible to use this new approach in order to measure, in an absolute way, the Newton coefficient h or the Nusselt Number Nu and thus, by using an appropriate correlation, the flow velocity v.

2.3.2.3. Conclusion

The modelling of a single wire, operating in the linear mode, in terms of a Laplace transfer function, allows for a new approach of the use of such a sensor, based on a frequency description. A new absolute method of fluid flow characterization has thus been developed using this approach. This new approach is also very fruitful in the domain of fluid thermal properties characterization.

2.3.3. Non linear mode of operation – The electrothermal analogy

2.3.3.1. Presentation

The preceding approach is limited to the description of the linear mode of operation of the single wire. In the common case of large variations in the temperature of the sensor, as for example in the case of the classical CTA or CCA modes, another approach is necessary to be able to realistically describe the operation of the sensor. The electrothermal analogy exposed

http://dx.doi.org/10.5772/60888

in the paragraph 2.2.3, is an interesting approach to illustrate the mode of operation of the hot wire resistive sensor, in the most general configuration.

If Ox denotes the axis of symmetry of the wire, the electrical circuit of Fig. 2b allows to describe the mechanisms of the instantaneous heat transfers between an infinitesimal volume $\mathrm{d}\tau$ of the wire and its environment, with $A_x = \pi d^2/4$, $A_{\text{lat}} = \pi d\mathrm{d}x$ and the Newton coefficient h is given by the correlation of Churchill and Bernstein [12], which is known for its universality over a wide range of flow conditions:

$$h(v_\infty) = \frac{k_f}{2a_1}\left\{0.3 + \frac{0.62\ \mathrm{Re}^{1/2}\mathrm{Pr}^{1/3}}{\left[1+\left(\frac{0.4}{\mathrm{Pr}}\right)^{2/3}\right]^{1/4}}\left[1+\left(\frac{\mathrm{Re}}{282000}\right)^{5/8}\right]^{4/5}\right\} \tag{24}$$

where $\mathrm{Re} = dv/\nu_f$ and $\mathrm{Pr} = \nu_f/\kappa_f$ are respectively the Reynolds and Prandtl numbers, ν_f is the kinematic viscosity, k_f the thermal conductivity and κ_f the thermal diffusivity of the fluid. This relation is valid as long as $\mathrm{Pr} \times \mathrm{Re} \geqslant 0.2$.

The wire is mathematically divided in N identical infinitesimal volumes, each of them being described by a circuit of the type 2b, that are connected in serial. Dirichlet boundary conditions are supposed at the extremities $x = \pm\ell/2$ of the system, due to the isothermal supports. The figure 10 shows such a modelling of the wire in term of the electrothermal analogy of table 1, for the elementary case where $N = 2$. Based on this circuit, a SPICE code allows to calculate the instantaneous voltages $U_i^T(t)$, analogous to the temperatures $T_i(t)$ of each elementary volume.

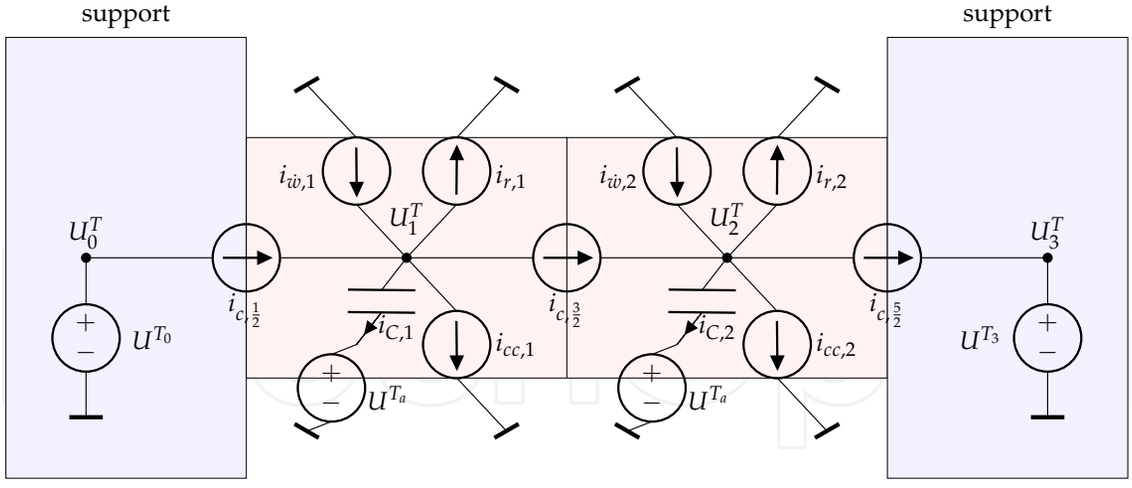

Figure 10. Electrothermal circuit equivalent to the hot wire sensor. For reasons of space and clarity, the model has been restricted to $N = 2$.

The simulated wire is supposed to be made of platinum, with a length $\ell = 1$ cm and a diameter $d = 10\,\mu$m. Its resistance at room temperature is $R_{\mathrm{w},a} = 13.58\,\Omega$. If for example we choose to impose a value of the resistance $\overline{R}_{\mathrm{w}} = 22\,\Omega$ by setting $R_1 = 22\,\Omega$ in the CTA circuit, the average temperature of the wire should consequently be $\delta\overline{T}_{\mathrm{w}} = 159.5$ K, whatever

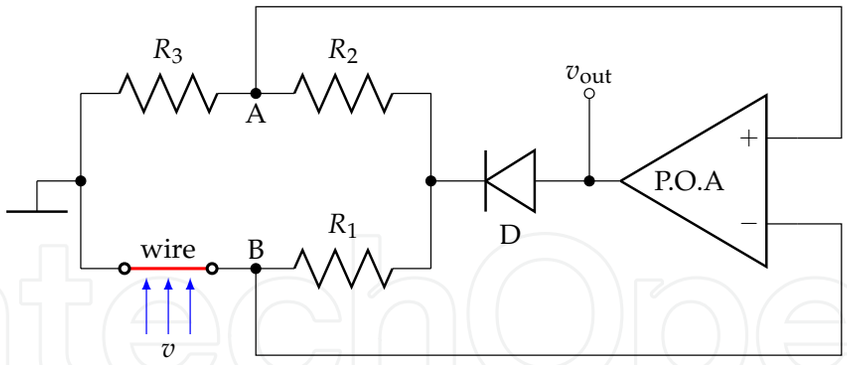

Figure 11. Elementary CTA circuit. D is a signal diode (1N4148), P.O.A is a power operational amplifier (OPA 548), $R_2 = R_3$ and are of the order of 1 kΩ. The value of R_1 is chosen in order to control the value of the resistance $\overline{R}_w$ of the wire and consequently its temperature $\overline{T}_w$. The output v_{out} is a function of the flow velocity v.

the velocity of the fluid around the wire. To test the quality of the present electrothermal analogy, we decide to impose important harmonic variations of the fluid velocity $v(t) = v_{c,0} + \hat{v}\cos\omega t$ where $\nu = \omega/2\pi = 10$ Hz, $v_{c,0} = 2.5\,\text{m.s}^{-1}$ and $\hat{v} = 1.5\,\text{m.s}^{-1}$, which means 60% in variations (Fig. 12). As we can see from the results of the simulation, the temperature of the wire is stabilized at around 0.2% of its average value, while its resistance is stabilized at 0.08% of its average value $\overline{R}_w$. We have also plotted in figure 13, the evolution of the output

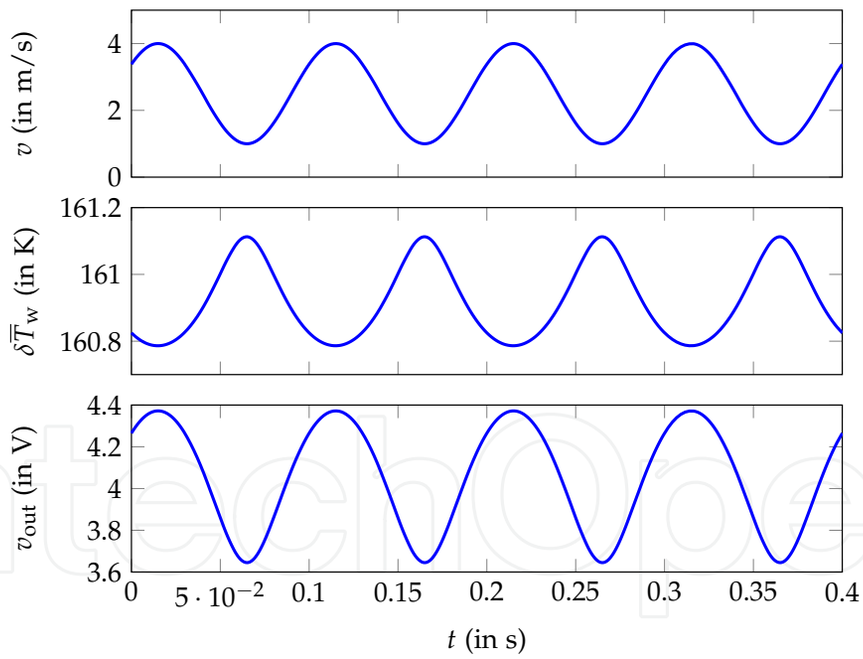

Figure 12. Results of the simulation of a CTA circuit, using an electrothermal analogy of a hot wire sensor.

v_{out} as a function of the velocity of the fluid v. This curve is typical of the evolution of the coefficient of transfer h with the fluid velocity v, showing once more the good adequacy of this approach with the description of the CTA mode. It is also possible to add some noise to the velocity v and thus to test the stability of the model. The obtained results, not reported here, show a very good behavior of the modelling in respect to the noise.

http://dx.doi.org/10.5772/60888

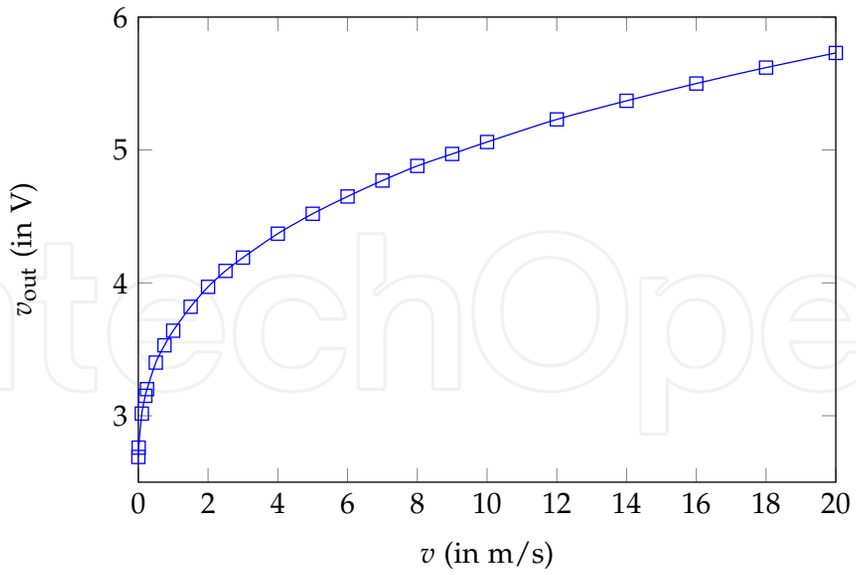

Figure 13. Results of the simulation of a CTA circuit, using an electrothermal analogy of a hot wire sensor.

2.3.3.2. Conclusion

The approach in term of an electrothermal analogy is a very powerful modelling tool, allowing to realistically describe the different modes of operation of a hot wire sensor. This opens the way to a systemic description of the whole system: sensor, control and signal processing electrical circuits. A Python script is available, upon request to the author (at the following address: rodolphe.heyd@cnrs-orleans.fr). It allows to generate a SPICE sub-circuit that is equivalent to the whole wire, with an arbitrary number N of infinitesimal volumes, under Dirichlet boundary conditions. SPICE scripts describing the operation of a CTA, based on the present modelling, are also available.

2.4. Resistive flat film sensor

2.4.1. Presentation – Mathematical model

The miniature thin-film resistive sensors (see Fig. 1) are very commonly used to measure the temperature, in many applications ranging from biomedical instrumentation to automotive industry or cooling systems for example. In most of the cases, the sensitive resistive film is protected by insulating shells and maintained on the system to study by an adhesion layer. These sensors are thus composite systems (see Fig. 14) and due to the heat conduction process through the different layers, the instantaneous operating temperature provided by the sensor can be different from that to be measured.

In order to take into account the influence of the different constitutive layers on the operation of the sensor, we first need to solve the problem of heat conduction through the sensor. As in the case of the single wire, we will first use the formalism of the Laplace transform. This allows us to provide an analytical expression of the distribution of the temperature in the system as a continuous function of the position and the time. This analytical approach also has the advantage to clearly identify the influence of the different physical parameters on the behavior of the system, thus facilitating its optimization for example. Moreover this

formalism allows to describe the thermal behavior of the composite system in terms of transfer functions [8, 10, 11], allowing inverse analysis.

In order to obtain a realistic modelling of the flat thin film sensor, we have to consider the conduction of heat through a thin composite slab (see Fig. 14) of finite thickness $L_2 + L_1 \approx$ 100 to 500 μm. The bottom layer (1) is frequently made of ceramic while the top layer (2) is usually a very thin passivation coating, made of glass. The thickness 2ϵ of the metallic film (h) is only a fraction of that of the coating layers and is of the order of 10 to 100 nm. The lateral dimensions a and b of the slab are frequently of the order of a few millimeters to a few centimeters. Therefore we can consider that the heat transfer inside this composite system is only axial. It is also possible to use flexible sensors, for which the sensing metallic film is protected by two polyimide layers for example.

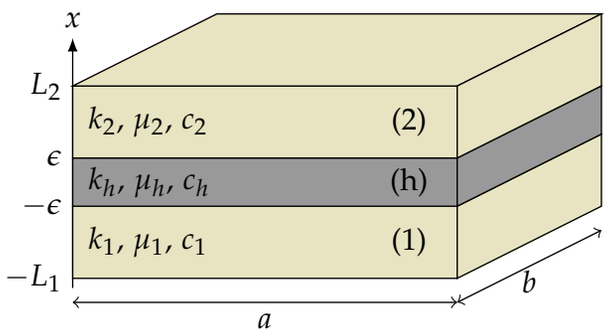

Figure 14. Composition of the composite slab considered in this study, with $L_j \ll a, b$ and $\epsilon \ll L_j$ where $j = 1, 2$.

We assume that the very thin metallic film has a high thermal conductivity k_h and is inserted between two insulating materials with thermal conductivity $k_j \ll k_h$, where $j = 1, 2$. The imperfect thermal contacts, between the very thin film and the insulating shells, are modeled by introducing thermal contact resistances. Because of the dimensions of the slab ($L_j \ll a, b$) and of the boundary conditions considered here, a planar invariance (no dependence in y and z) without in-plane temperature gradients is supposed. It follows that the temperature $T(x,t)$ of the slab is a function of x and t only, written as $T(x,t) = T_a + \delta T(x,t)$. At initial time $t = 0$, the whole system is supposed to be at thermal equilibrium with an uniform temperature T_a, therefore $\delta T(x,0) = 0$. For time $t > 0$, we consider heat conduction through the whole system due both to the outermost boundary conditions, at $x = L_2$ and $x = -L_1$, and to internal heat sources supposed to be localized only inside the high conductivity film (h). This heat conduction induces temperature variations $\delta T_j(x,t)$ of the coatings that satisfy the following one-dimensional diffusion equations:

$$\partial_t \left[\delta T_j(x,t)\right] = \alpha_j \partial_{x^2} \left[\delta T_j(x,t)\right] \tag{25}$$

where $\alpha_j = k_j / \mu_j c_j$ is the thermal diffusivity, μ_j is the density and c_j is the specific heat of the corresponding coating, that are supposed constant in the linear approach considered here. Under these conditions, the differential operator $L_{x,j}(t)$ of equation (1) is simply written as $L_{x,j}(t) = \partial_{x^2}$, with $j \neq h$.

http://dx.doi.org/10.5772/60888

Moreover, due to the high value of the ratio k_h/k_j commonly encountered with resistive sensors, the temperature $T_h(x,t) = T_a + \delta T_h(x,t)$ of the high thermal conductivity film can be considered as uniform to a very good approximation. Numerical simulations, made with the finite element solver FlexPDE, show that in all the cases under study here, the spatial variations in the temperature $\delta T_h(x,t)$ are absolutely negligible: $1 - |\delta T_h(0,t)/\delta T_h(\pm\epsilon,t)| < 0.1\%$. Thus it is possible to consider that the temperature δT_h only depends on the time t. Therefore the energy balance of the highly conductive film can be written as:

$$2\epsilon ab\mu_h c_h \frac{\mathrm{d}\delta T_h}{\mathrm{d}t} = \dot{Q}_h + \dot{W}_h \tag{26}$$

where $\dot{W}_h(t)$ is the internal heat power due to the Joule effect and $\dot{Q}_h(t) = \dot{Q}_{h,\epsilon}(t) + \dot{Q}_{h,-\epsilon}(t)$ is the heat exchanged by unit time between the sensing film (h) and the insulating shell. The temperature uniformity of the highly conductive film and the introduction of the thermal contact resistances, allow us to write at $x = \pm\epsilon$:

$$\delta T_h(t) = \delta T_1(-\epsilon,t) - R_1^c \dot{Q}_{h,-\epsilon}/ab = \delta T_2(\epsilon,t) - R_2^c \dot{Q}_{h,\epsilon}/ab \tag{27}$$

where R_1^c and R_2^c are the thermal contact resistances respectively at $x = -\epsilon$ and $x = \epsilon$. Furthermore, the continuity of the heat fluxes at $x = \pm\epsilon$ leads to the following relations:

$$ab\,k_1 \left(\frac{\partial \delta T_1}{\partial z}\right)_{-\epsilon} = -\dot{Q}_{h,-\epsilon}(t) \;\text{ and }\; ab\,k_2 \left(\frac{\partial \delta T_2}{\partial z}\right)_{\epsilon} = \dot{Q}_{h,\epsilon}(t) \tag{28}$$

In the limit of a very thin conductive film that is considered here, $\epsilon \ll L_j$, it is possible to neglect the term $2\epsilon ab\mu_h c_h \mathrm{d}\delta T_h/\mathrm{d}t$ compared to $\dot{Q}_h$ and $\dot{W}_h$. Thus we can write with a very good approximation:

$$\dot{W}_h(t) = -\left[\dot{Q}_{h,\epsilon}(t) + \dot{Q}_{h,-\epsilon}(t)\right] \tag{29}$$

In order to find the time evolutions of the temperatures δT_j and δT_h, we first apply the Laplace transform to the equations (25), (27), (28) and (29), we obtain:

$$sF_j = \alpha_j \partial_{x^2} F_j \tag{30}$$

$$F_h(s) = F_1(-\epsilon,s) - R_1^c \dot{q}_{h,-\epsilon}(s) = F_2(\epsilon,s) - R_2^c \dot{q}_{h,\epsilon}(s) \tag{31}$$

$$k_1 \left(\partial_x F_1\right)_{-\epsilon} = -\dot{q}_{h,-\epsilon}(s) \;\text{ and }\; k_2 \left(\partial_x F_2\right)_{\epsilon} = \dot{q}_{h,\epsilon}(s) \tag{32}$$

$$\dot{w}_h(s) = -\left[\dot{q}_{h,\epsilon}(s) + \dot{q}_{h,-\epsilon}(s)\right] \tag{33}$$

where $F_j(x,s)$, $F_h(s)$, $\dot{w}_h(s)$ and $\dot{q}_{h,\pm\epsilon}(s)$ are the Laplace transforms respectively of $\delta T_j(x,t)$, $\delta T_h(t)$, $\dot{W}_h(t)/ab$ and $\dot{Q}_{h,\pm\epsilon}(t)/ab$. The solutions of the equations (30) can be written as:

$$F_j(x,s) = A_j(s)e^{\chi_j x} + B_j(s)e^{-\chi_j x} \tag{34}$$

where $\chi_j^2 = s/\alpha_j$. Using the continuity relations (31) and (32) ; the internal constraint (33) together with the outermost boundary conditions located at $x = -L_1$ and $x = L_2$, it is possible to find the expressions of the six unknowns $A_1(s)$, $A_2(s)$, $B_1(s)$, $B_2(s)$, $\dot{q}_{h,\epsilon}(s)$ and $\dot{q}_{h,-\epsilon}(s)$. Finally by reversing the relation (34), we can find the time evolution of the temperatures and heat fluxes at each point of the system, according to the boundary conditions and internal heat source considered.

2.4.2. Temperature sensor mode

2.4.2.1. Dirichlet boundary conditions and transfer function

In usual situations, the highly conductive film is the sensing element whose operating temperature $\delta T_h(t)$ is measured and controlled. We want to determine here the evolution of this temperature as a function of the outermost temperatures of the sensor: $\delta T_1(-L_1, t) = \delta T_1(t)$ and $\delta T_2(L_2, t) = \delta T_2(t)$. Applying the Laplace transform to these Dirichlet boundary conditions, we get:

$$F_1(-L_1, s) = X_1(s) \tag{35}$$

$$F_2(L_2, s) = X_2(s) \tag{36}$$

where X_1 and X_2 are the Laplace transforms respectively of $\delta T_1(t)$ and $\delta T_2(t)$.

In order to deduce the real-time evolution of $\delta T_h(t)$ from the knowledge of the boundary temperatures $\delta T_1(t)$ and $\delta T_2(t)$, we need first to find the relationship between $F_h(s)$, $X_1(s)$ and $X_2(s)$. To simplify the mathematical expressions further, without reducing the generality of this approach, the system is assumed to be symmetric according to the plane $x = 0$. Using the relations (31) to (36) we get the following expression:

$$F_h(s) = \dot{w}_h(s) \left[\frac{\tanh\left[(L-\epsilon)\sqrt{s/\alpha}\right]}{2k\sqrt{s/\alpha}} + \frac{R^c}{2} \right] + \frac{X_1(s) + X_2(s)}{2\cosh\left[(L-\epsilon)\sqrt{s/\alpha}\right]} \tag{37}$$

where $L = L_j$, $\alpha = \alpha_j$, $k = k_j$ and $R^c = R_j^c$, with $j = 1, 2$. As mentioned earlier in this section, it may be important to be able to quantify the influence of the internal self-heating on the temperature measurements using thin-film resistive sensors. The expression (37) clearly answers this question by showing the influence of the boundary temperatures X_1 and X_2 separately from the influence of the internal heat source $\dot{w}_h$.

It is still possible in the present case, to describe the sensor in terms of a combination of two linear dynamical systems as shown in Fig. 15, where H_X and H_w are the Laplace transfer functions associated respectively with the outermost boundary temperatures and the internal heat source, and defined by:

$$H_X(s) = 1/\cosh\left[(L-\epsilon)\sqrt{s/\alpha}\right] \tag{38}$$

$$H_w(s) = \frac{\tanh\left[(L-\epsilon)\sqrt{s/\alpha}\right]}{2k\sqrt{s/\alpha}} + \frac{R^c}{2} \tag{39}$$

http://dx.doi.org/10.5772/60888

The relation (37) can now be written as:

$$F_h(s) = H_w(s)\dot{w}_h(s) + H_X(s)\frac{X_1(s) + X_2(s)}{2} \tag{40}$$

$$= F_{hX}(s) + F_{hw}(s) \tag{41}$$

Returning to the real time space, the operating temperature of the sensor can thus be written as $\delta T_h(t) = \delta T_{hX}(t) + \delta T_{hw}(t)$, where $\delta T_{hX}(t)$ is the contribution due to the outermost temperatures of the sensor and $\delta T_{hw}(t)$ is the contribution due to the internal heat source.

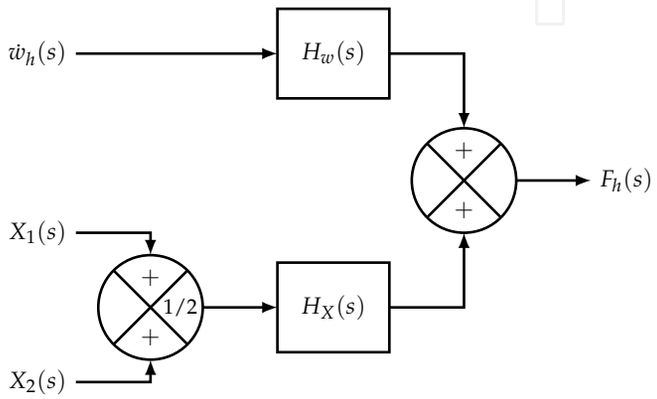

Figure 15. Description of the thin film sensor using a combination of two linear systems.

The inverse Laplace transform of the relation (37) must be computed now, in order to obtain the time variations of the temperature δT_h. Depending on the time evolutions of both the internal heat source and of the boundary temperatures, an analytical inversion of the Laplace transform $F_h(s)$ is not always possible. It is therefore essential to be able to reverse the function $F_h(s)$ in an approximate way, but with a sufficient accuracy to allow a precise description of the complete time evolution of the physical quantities, from the initial transient regime until the steady state.

There are usually several ways to calculate $\delta T_h(t)$ based on the relation (37). When the analytical expressions of the functions $\dot{w}_h(t)$, $\delta T_1(t)$ and $\delta T_2(t)$ are known, it is possible to resort to numerical Laplace transform inversion schemes [13–15]. However, this method becomes very difficult to apply when the temperatures $\delta T_1(t)$ and $\delta T_2(t)$ are known only as a set of discrete values provided for example by experimental records. Moreover, in the temperature measurement mode, these outermost temperatures are usually unknown or at the best partially known. We prefer to apply a method developed in [11], that uses the Padé digital filters. This approach presents the great advantages on the one hand to not require a Laplace inversion and on the other hand to allow to consider realistic situations, where the outermost temperatures and the source term are given for example by experimental records.

The first step of this method consists in approximating the Laplace transfer functions $H(s)$ by precise rational functions, obtained by using their Padé approximants, and expressed in the form:

$$H^{\mathrm{PA}}(s) = \frac{H(0) + \sum_{k=1}^{M} b_k s^k}{1 + \sum_{k=1}^{N} a_k s^k} \tag{42}$$

where the coefficients $\{a_k, b_k\}$ are calculated analytically using the following equality [16]:

$$\frac{\mathrm{d}^k}{\mathrm{d}s^k} H^{\mathrm{PA}}(s)\bigg|_{s=0} = \frac{\mathrm{d}^k}{\mathrm{d}s^k} H(s)\bigg|_{s=0}, \; k = 1, 2, \ldots, M+N \tag{43}$$

Next we determine the digital filter corresponding to $H(s)$ by applying the bilinear transformation $s = \frac{2}{T_e}\frac{Z-1}{Z+1}$, where T_e is an appropriate sampling period [17]. After some algebra manipulations, we obtain an approximated Z transfer function of the form:

$$H^{\mathrm{PA}}(Z) = \frac{\sum_{k=0}^{M} A_k Z^{-k}}{1 + \sum_{k=1}^{N} B_k Z^{-k}} \tag{44}$$

where the coefficients (A_k, B_k) are expressed as a function of the sampling period T_e and coefficients (a_k, b_k) that are deduced from the relation (43). Finally we deduce from (44), a recursion formula that is easy to calculate using sampled quantities. To illustrate this process, we consider for example the situation where both faces of the sensor are submitted to the same temperature variations: $\delta T_1(t) = \delta T_2(t) = \delta T_X(t)$, $X_1(s) = X_2(s) = X(s)$ and $F_{hX}(s) = H_X(s)X(s)$, where $H_X(s)$ is given by (38). This is the case for example when the sensor is immersed at initial time $t = 0$ in a turbulent liquid or put in perfect thermal contact with a thermostat.

From the Padé Z transfer function $F_{hX}^{\mathrm{PA}}(Z)$ we can deduce the recursion relation satisfied by the component T_{hX} of the sensing element temperature:

$$\delta T_{hX}(nT_e) = \sum_{k=0}^{M} A_k \delta T_X((n-k)T_e) - \sum_{k=1}^{N} B_k \delta T_{hX}((n-k)T_e) \tag{45}$$

The same procedure holds for the internal heat source contribution δT_{hw}:

$$\delta T_{hw}(nT_e) = \sum_{k=0}^{M} A'_k \dot{w}_h((n-k)T_e) - \sum_{k=1}^{N} B'_k \delta T_{hw}((n-k)T_e) \tag{46}$$

where the coefficients (A'_k, B'_k) are deduced from the approximated Padé transfer function H_w^{PA}.

http://dx.doi.org/10.5772/60888

2.4.2.2. Influence of self-heating

To illustrate the benefit of the approach in terms of Laplace transfer functions, using the relation (37) together with the associated discrete digital Padé filters (45 and 46), we can compute the real-time evolution of the temperature $\delta T_h(t)$ in the case of a non-negligible contribution of the internal heat source. The results have been compared with those provided by the finite elements (FE) solver FlexPDE.

The physical characteristics of the thin film sensor considered in the following calculations are: $L = 30\,\mu$m, $\epsilon = 1.0\,\mu$m, $a = b = 1$ mm, $k = 0.12\,\mathrm{W.K^{-1}.m^{-1}}$, $\tau^{-1} = \alpha/(L-\epsilon)^2 = 89.1$ Hz and $R_{h,a} = 10\,\Omega$. The influence of the thermal contact resistances has been taken into account using a typical value of $R^c = 2.0 \times 10^{-4}\,\mathrm{W^{-1}.m^2.K}$. The sampling period used with the digital Padé filters is chosen equal to $T_e = 0.05/\tau$.

We consider first the case of a sudden variation of the boundary temperature $\delta T_X(t) = \delta T_X^m \Theta(t)$, together with a constant internal heat source $\dot{w}_h(t) = \dot{w}_h^m \Theta(t)$, where $\delta T_X^m = 1\,$K ; $\dot{w}_h^m = 4 \times 10^3\,\mathrm{W/m^2}$ and $\Theta(t)$ is the Heaviside step function. As shown in Fig. 16, the curve representing the real-time evolution of the temperature δT_h, calculated using the Padé digital filters, is nearly undistinguishable from that obtained using the FE solver (circles). The Fig. 16 shows that the relation (13) also presents the advantage, compared to the use of a FE solver, to allow for the calculation of the real-time contribution of the boundary temperatures δT_X separately from that of the internal heat source. In the particular case of a resistive sensor, this approach could permit a real time evaluation of the modelling of the influence of the self-heating on the accuracy of the outermost temperature measurements.

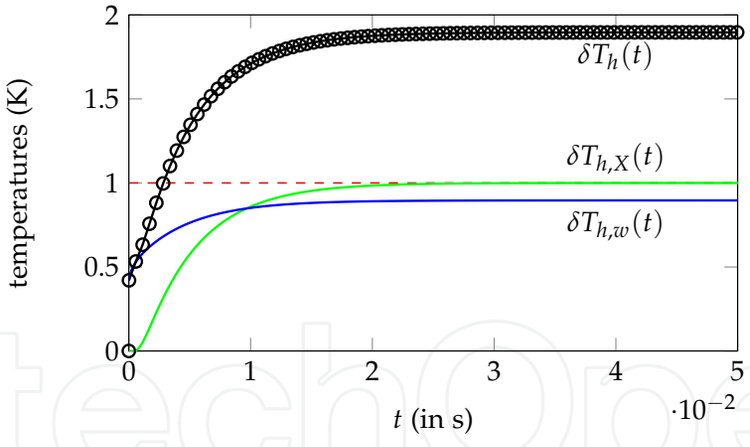

Figure 16. Time evolution of the operating temperature δT_h of a miniature thin film resistive sensor, in the case of a non-negligible contribution of the internal heat source, calculated by using Padé digital filters and a FE solver (circles). The curves show the decomposition of the operating temperature thanks to the transfer function approach: $\delta T_h = \delta T_{hX} + \delta T_{hw}$. The dashed line corresponds to the outermost temperature δT_X to be measured.

2.4.2.3. Inverse analysis

The direct analysis presented earlier is of a great interest in order to model the operation of the sensor but it is also very interesting to be able to process the thermal signal $\delta T_h(t)$ provided by the sensor in real time, in order for example to recover a precise estimate of the outermost temperatures, in spite of the self-heating. This is an inverse heat conduction

problem, where the influence of self-heating must be corrected. By rewriting the relation (37) as:

$$X(s) = H_X^{-1}(s)F_h(s) - H_X^{-1}(s)H_w(s)\dot{w}_h(s) \tag{47}$$

with $H_X^{-1} = 1/H_X$, it is now possible to determine the boundary temperature $\delta T_X(t)$ from the knowledge of $\delta T_h(t)$ and $\dot{w}_h(t) = \dot{W}_h(t)/ab$. We also use the method of the digital Padé filters to solve this inverse problem. It is possible to construct digital filters based on Padé approximants of the transfer functions $G_X = H_X^{-1}$ and $G_w = H_X^{-1}H_w$. These functions have a pathological behavior since they diverge when s diverges, so it is very unlikely to find some approximations of G_X and G_w by rational functions, that would allow for a stable resolution of this inverse problem. To overcome this difficulty, we approximate the functions G_f by the following rational functions, with f denoting X or w:

$$G_f^M(s) = \frac{G_f(0) + \sum_{k=1}^{M} b_k s^k}{1 + \sum_{k=1}^{M} a_k s^k} \tag{48}$$

where the b_k are the Padé coefficients of the function G_f, defined by the relation (43) with $N = 0$, but the a_k coefficients are chosen here in such a way that on the one hand $a_k \ll 1$ and on the other that the Routh–Hurwitz stability criterion is satisfied. With these choices, the rational function G_f^M allows for the stability of the inverse problem while being very close to the Padé approximant $G_f^{M,0}$ of G_f.

This inverse analysis is illustrated now by considering a situation where the outermost temperature $\delta T_X(t)$ is described by a square wave, the self-heating is considerable and the operating temperature $\delta T_h(t)$ is noisy, due for example to experimental conditions (Figure 17). The stability of the inverse Padé digital filter is not disturbed by the abrupt changes generated by the outermost temperature discontinuities and the Gaussian noise added to the exact operating temperature. If needed, the reconstructed outermost temperature can be filtered to smooth the unwanted residual noises. As can be seen on Fig. 17, the successive operations of inverse analysis and filtering allow for a good reconstruction (circles) of the outermost temperature $\delta T_X(t)$ (dashed line).

2.4.2.4. Extreme conditions

We have previously considered situations where the temperature variations were limited to only a few Kelvins (Fig. 16 and 17), thus the corresponding variations of the resistance R_h of the sensor can be neglected in the expression of the heat source term $\dot{w}_h(t) = R_h\left[\delta T_h(t)\right] i^2(t)/ab \approx R_{h,a} i^2(t)/ab$. This assumption is usually well verified in the domain of biomedical applications for example. However, this type of sensor can also be used in more extreme applications where the temperature variations are so large that the value of the resistance R_h can no more be considered as constant within the source term $\dot{w}_h$. The use of recursive filters offers the possibility to consider the problem of such extreme temperature variations, with only a few modifications of the preceding approach. Through

http://dx.doi.org/10.5772/60888

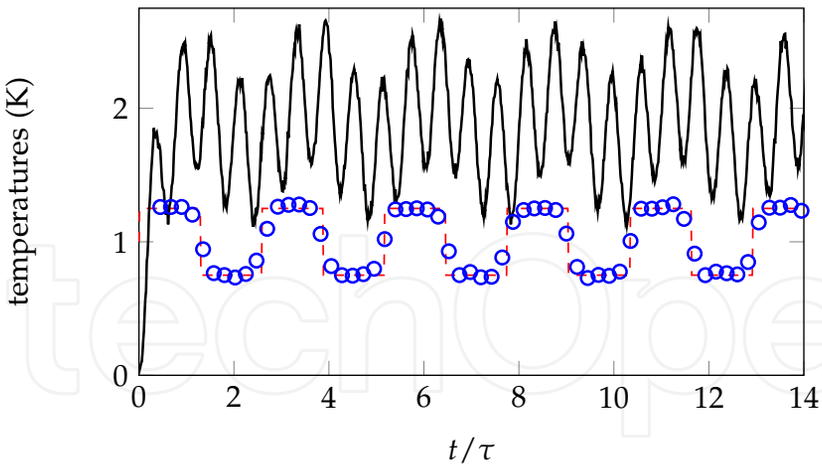

Figure 17. Time evolution of the operating temperature δT_h (solid line) in the case where the outermost temperature δT_X is a square wave (dashed line) and a Gaussian noise has been added to the operating temperature, with a 0 K mean value and a 0.03 K standard deviation value. The reconstructed δT_X is given by the circles.

the decomposition of the operating temperature as $\delta T_h = \delta T_{hX} + \delta T_{hw}$, we write first the source term $\dot{w}_h$ as:

$$\dot{w}_h(t) = \dot{w}_h^0(t)\left[1 + \alpha_m\left(\delta T_{hX}(t) + \delta T_{hw}(t)\right)\right] \tag{49}$$

with $\dot{w}_h^0(t) = R_{h,a} i^2(t)/ab$ and $\alpha_m = \alpha_h R_{h,\mathrm{ref}}/R_{h,a}$, where α_h is the temperature coefficient of the metallic film. Next we modify the recursion relation (46) in order to take into account the time evolutions of δT_{hX} and δT_{hw}:

$$\begin{aligned}\delta T_{hw}(nT_e) = &\sum_{k=0}^{M} A'_k \dot{w}_h^0((n-k)T_e)\left[1 + \alpha_m \delta T_{hX}((n-k)T_e) + \alpha_m \delta T_{hw}((n-k-1)T_e)\right] \\ &- \sum_{k=1}^{N} B'_k \delta T_{hw}((n-k)T_e)\end{aligned} \tag{50}$$

where the coefficients (A'_k, B'_k) are the same as those used in the relation (46) and $\delta T_{hX}((n-k)T_e)$ is still calculated using the relation (45), that must be solved first. Because of the recursive structure of (50), a small delay must be used in the expression of $\alpha_m \delta T_{hw}$.

To illustrate the efficiency of this approach, let's consider large outermost temperature variations $\delta T_X(t) = 250 \times (1 - \exp -t/\tau')$, together with a large contribution of the self-heating by using $R_{w,a} = 1000\,\Omega$, $i(t) = 0.014 \sin(2\pi\nu t)$ and a thermal contact resistance $R^c = 2.0 \times 10^{-4}\,\mathrm{W}^{-1}.\mathrm{m}^2.\mathrm{K}$.

Compared to the FEM results (dots) shown in the Figure 18a, the linear approach based on the recursion relation (46) gives very bad results in the present case . In contrast, we can see on Fig. 18b that the approach based on the modified recursion relation (50) gives excellent results (solid line), nearly undistinguishable from those found with a FEM solver. Another benefit of this approach is that the inversion relation (47) is still usable, even in the presence of this type of extreme temperature variations.

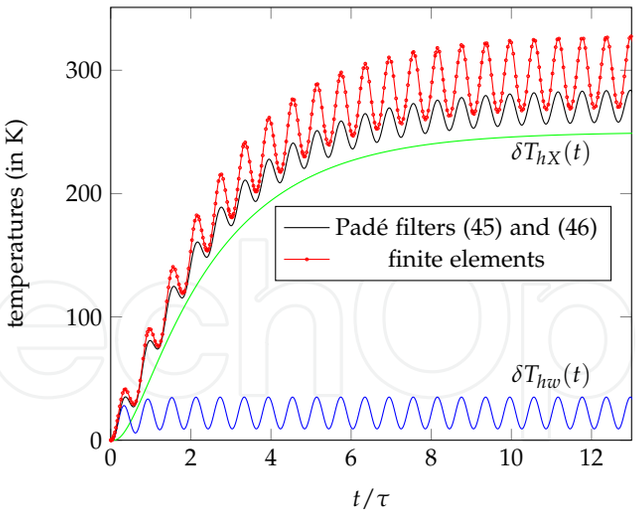

(a) Solution using the recursive filters (45) and (46). The results obtained here are very different from those obtained by finite element calculations (FEM).

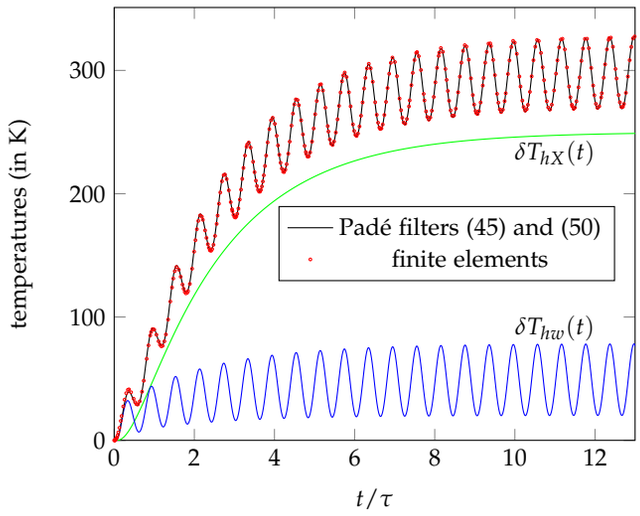

(b) Solution using the recursive filters (45) and (50). The results are now very closed to those obtained by FEM.

Figure 18. Thin film resistive sensor modeled by using Padé filters in the case of important variations of the temperatures.

2.4.2.5. Mixed boundary conditions

We consider now the frequent case of mixed boundary conditions. We suppose that the heat flux obeys the Newton's law of convective cooling at the position $x = L_2$: $-k_2 \left(\partial_x T_2\right)_{L_2} = h(T_2 - T_a)_{L_2}$, where h is the convective heat transfer coefficient and T_a is the temperature of the fluid, far from the sensor. At the bottom surface $x = -L_1$, we assume that the outermost temperature is known, due to a perfect thermal contact of the sensor with a solid of temperature $T_1(t) = \delta T_1(t) + T_a$. By applying the Laplace transform to these boundary conditions, together with the relations (31) to (36) and using the same assumption of symmetry as in the preceding sections, it is still possible to write $F_h(s) = H_X(s)X(s) + H_w(s)\dot{w}_h(s)$, where $X(s)$ is the Laplace transform of $\delta T_1(t)$, $H_X(s)$ and $H_w(s)$ are given here by:

http://dx.doi.org/10.5772/60888

$$H_X(s) = \frac{h \sinh\left[(L-\epsilon)\sqrt{s/\alpha}\right] + k\sqrt{s/\alpha}\cosh\left[(L-\epsilon)\sqrt{s/\alpha}\right]}{h \sinh\left[2(L-\epsilon)\sqrt{s/\alpha}\right] + k\sqrt{s/\alpha}\cosh\left[2(L-\epsilon)\sqrt{s/\alpha}\right]} \tag{51}$$

and

$$H_w(s) = \frac{\sinh\left[(L-\epsilon)\sqrt{s/\alpha}\right]}{k\sqrt{s/\alpha}} \times H_X(s) \tag{52}$$

We focus now on the analysis of the influence of some physical parameters on the overheating temperature [18] $\Delta T = T_h - T_1 = \delta T_h - \delta T_1$, rather than on the inverse analysis in the case of self-heating, study that is very similar to the previous one.

Let's consider a constant internal heat source of a typical value $\dot{w}_h = 4 \times 10^3\,\mathrm{W/m^2}$ and constant boundary conditions. From the study of the real-time evolution, obtained with the digital Padé filters deduced from transfer functions (51) and (52), we calculate the steady-state values of the overheating temperature of the thin film sensor previously described. These results are in good agreement with those provided by finite element calculations (FlexPDE solver) based on the geometric configuration illustrated by the Fig. 1b and 19a. The value of the operating temperature T_h has been considered at the center of the thin-film.

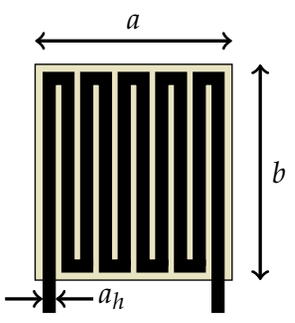

(a) Top view of the thin film sensor, $a = b = 1\,\mathrm{mm}$ and $a_h = 95\,\mu\mathrm{m}$. The lateral sides are supposed thermally insulated. The thin-film heater (h) is encapsulated by an isolating coating of width $2(L-\epsilon) \approx 2L$.

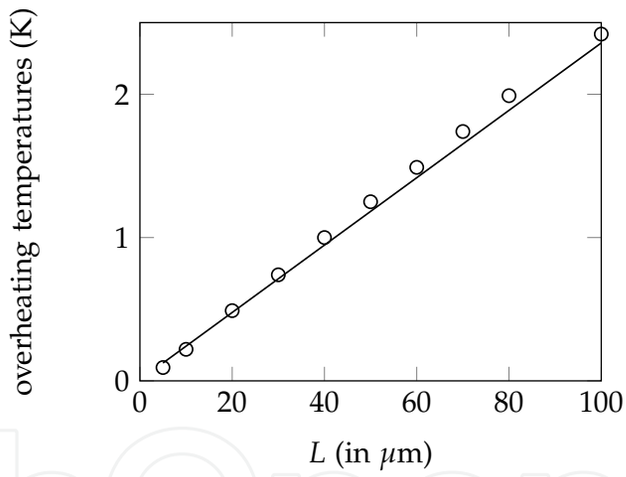

(b) Overheating temperature $\Delta T = T_h - T_1$ of the sensing film (h) as a function of the width L of the coating layers, $h = 100\,\mathrm{W.m^{-2}.K^{-1}}$ and $\delta T_1 = 10\,\mathrm{K}$.

Figure 19. Overheating study of the thin film sensor by using Laplace transfer functions.

The Fig. 19b shows a linear evolution of the steady-state overheating temperature within the considered range of values of the thickness L. As expected, the overheating temperature increases with the thickness of the insulating coating. The influence of other parameters (such as h, δT_1, k, μ) can easily be studied in the same way with this method [11], at a fraction of the time needed with a FEM calculations, while having the advantage of an analytical approach.

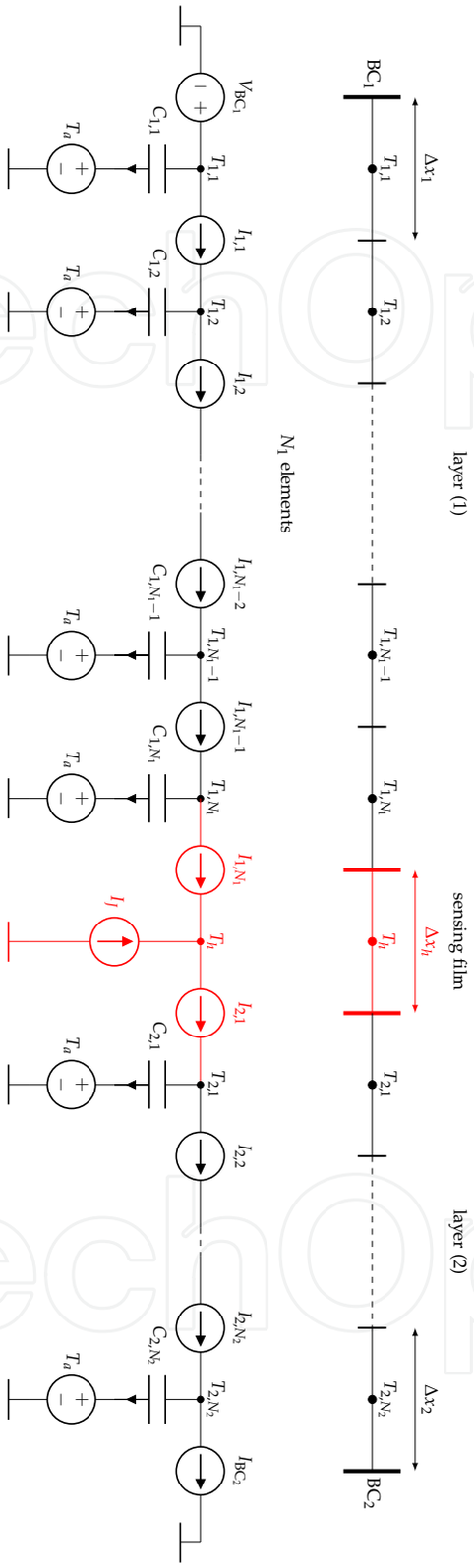

Figure 20. Electrothermal model equivalent to a non-symmetrical resistive thin film sensor. The boundary condition at $x = -L_1$ is of Dirichlet type, whereas the boundary condition at $x = L_2$ is of Robin type.

2.4.2.6. Electrothermal analogy

As in the case of the single wire sensor, an electrothermal analogy can be proposed in the case of the thin film sensor. It allows to easily consider the systemic modelling of nonlinear or non-symmetrical situations. Considering that the heat transfer through the lateral sides of the sensor is negligible compared to the parietal transfer, the general electrothermal analogy of paragraph 2.2.3 is formulated in the present case, as shown in Fig. 20. The boundary conditions considered in this example are the following: Dirichlet conditions at $x = -L_1$ and Robin (or mixed) conditions at $x = L_2$. This sub-circuit allows to simulate the operation mode considered in the paragraph 2.4.2.5.

Upon request to the author, a Python script is available, that allows the generation of a SPICE sub-circuit that is equivalent to the whole thin-film sensor, with an arbitrary number of infinitesimal volumes, under arbitrary boundary conditions.

3. Conclusion

We have exposed in this chapter two very rich and complementary approaches of the modelling of resistive electrothermal sensors. The first one uses the Laplace transform in order to allow a modelling of the sensor in terms of transfer functions. This opens the way to new modes of utilization of the electrothermal sensors, such as the absolute anemometry or thermal characterization of materials. This approach also allows to develop inverse analysis methods, in order for example to better consider and compensate the influence of the self-heating on the accuracy of thermal measurements using resistive sensors. The second approach exposed here uses an electrothermal analogy inspired from the Godunov scheme. It allows to consider more extreme situations than those considered by the transfer functions approach and also to envisage systemic approaches of the modes of operation of the resistive electrothermal sensors. This could be of great help to the designers of new instrumentation apparatus in the field of thermal measurement and materials and flow characterization. The same processes of modelling may be applied in the same way to the NTC resistive sensors made of semiconductors.

Author details

Rodolphe Heyd

ICMN UMR7374 CNRS/Orléans University, France

References

[1] Bruun, H. Hot-Wire Anemometry, Principles and Signal Analysis. *Oxford University Press, New-York*, (1995).

[2] Heyd, R., Hadaoui, A., Fliyou, M., Koumina, A., Ameziane, E., Outzourhit, A. and Saboungi. M. L. Development of absolute hot-wire anemometry by the 3ω method, *Review of Scientific Instruments* 81: 044901-1–044901-6, (2010).

[3] Silvestri, S. and Schena, E. Micromachined flow sensors in biomedical applications. *Micromachines*, 3:225–243, (2012).

[4] D'Aleo, F. P. and Prasser, H.-M. Design, calibration and testing of a thin film temperature gauge array for temperature and heat flux measurements in fluid mixing experiments, *Flow Measurement and Instrumentation*, 24:29–35, (2012).

[5] Cahill, D. Thermal conductivity measurement from 30 to 750 K: the 3ω method, *Review of Scientific Instruments*, 61: 802, (1990).

[6] Olson, B. W., Graham, S. and Chen, K. A practical extension of the 3ω method to multilayer structures, *Review of Scientific Instruments*, 76: 053901, (2005).

[7] Lee, S.-M. Thermal conductivity measurement of fluids using the 3ω method, *Review of Scientific Instruments*, 80: 024901, (2009).

[8] Feng, Z., Chen, J. and Zhang, Y. Real-time solution of heat conduction in a infinite slab for inverse analysis. *International Journal of Thermal Sciences*, 49:762–768, (2010).

[9] Feng, Z., Chen, J., Zhang, Y. and Montgomery-Smith, S. Temperature and heat flux estimation from sampled transient sensor measurements, *International Journal of Thermal Sciences*, 49:2385–2390, (2010).

[10] Heyd, R., Hadaoui, A. and Saboungi, M.-L. 1D analog behavioral Spice model for hot wire sensors in the continuum regime. *Sensors and Actuators A: Physical*, 174:9–15, (2012).

[11] Heyd, R. Real-time heat conduction in a self-heated composite slab by padé filters. *International Journal of Heat and Mass Transfer*, 71:606–614, (204).

[12] Churchill, S. W. and Bernstein, M. *Journal of Heat Transfer*, 94:300, (1997).

[13] Crump, K. S. Numerical inversion of Laplace transform using Fourier series approximation. *J. Assoc. Comput. Mach.*, 23:89–96, (1976).

[14] Durbin, F. Numerical inversion of Laplace transforms: an efficient improvement to Dubner and Abate's method. *The Computer Journal*, 17(4):371–376, (1973).

[15] Talbot, A. The accurate numerical inversion of Laplace transform. *J. inst. Maths. Applics.*, 23:97–120, (1979).

[16] Baker, G. A. J. and Graves-Morris, P. Padé Approximants. *Cambridge University Press, New York, second edition*, (1996).

[17] Ambardar, A. Analog and Digital Signal Processing. *Brooks/Cole, second edition*, (1999).

[18] Kozlov, A. G. Analytical modelling of temperature distribution in resistive thin-film thermal sensors. *International Journal of Thermal Sciences*, 45:41–50, (2006).